Experimental Observation of Quantum Talbot Effects

Xin-Bing Song,[1] Hai-Bo Wang,[1] Jun Xiong,[1] Kaige Wang,[1] Xiangdong Zhang,[1,*] Kai-Hong Luo,[2] and Ling-An Wu[2]

[1]*Department of Physics, Applied Optics Beijing Area Major Laboratory, Beijing Normal University, Beijing 100875, China*

[2]*Laboratory of Optical Physics, Institute of Physics and Beijing National Laboratory for Condensed Matter Physics, Chinese Academy of Sciences, Beijing 100190, China*

(Received 2 February 2011; revised manuscript received 12 June 2011; published 14 July 2011)

We report the first experimental observation of quantum Talbot effects with single photons and entangled photon pairs. Both the first- and second-order quantum Talbot self-images are observed experimentally. They exhibit unique properties, which are different from those produced by coherent and incoherent classical light sources. In particular, our experiments show that the revival distance of two-photon Talbot imaging is twice the usual classical Talbot length and there is no net improvement in the resolution, due to the near-field effect of Fresnel diffraction, which is different from the case of previous proof-of-principle quantum lithography experiments in the far field.

DOI: 10.1103/PhysRevLett.107.033902 PACS numbers: 42.30.Va, 42.50.Dv, 42.50.St

The Talbot effect is a near-field diffraction phenomenon in which self-imaging of a grating or other periodic structure replicates at certain imaging planes without the need for a lens [1]. The regular distance between the object and the imaging plane is called the Talbot length [2], $z_T = 2d^2/\lambda$, where d and λ are the period of the structure and the wavelength of the incident light, respectively. The effect has found interesting applications in image processing and synthesis, photolithography, optical testing, optical metrology, and spectrometry [3]. Recently, the phenomenon has also been demonstrated in areas such as atomic waves [4–6], waveguide arrays [7], x-ray phase imaging [8], and nonlinear systems [9].

Classical Talbot self-imaging is a kind of first-order imaging, which is encountered when a periodic object is illuminated with coherent light. Recently, second-order Talbot self-imaging with pseudothermal light has been observed experimentally [10,11]. The conditional Talbot effect and the second-order quantum Talbot effect with entangled photon pairs have been discussed theoretically by various research groups [12–14]. However, such quantum Talbot images have not been observed experimentally so far, although many other types of quantum imaging have been discussed and demonstrated [15–18]. Quantum imaging is expected to have extensive applications in quantum information and technology. For example, it has been demonstrated that it may be useful in quantum lithography [16,17], because of a possible breakthrough in lithographic resolution by overcoming the diffraction limit.

Here we report the first experimental observation of quantum Talbot imaging with entangled photon pairs. We first consider the case of single photons. An outline of the experimental setup is shown at the top of Fig. 1. The single photons are provided by the signal photons of photon pairs produced through spontaneous parametric down-conversion in a $5 \times 5 \times 3$ mm beta-barium-borate (BBO) crystal cut for type-I phase matching. The crystal is pumped by the second harmonic of a Ti:sapphire femtosecond laser (Mira-900 Coherent Inc.) with center wavelength $\lambda = 400$ nm, beam diameter 3 mm, and repetition rate 76 MHz. The signal photons pass through a single slit to improve the spatial coherence and then are detected after transmission through a one-dimensional rectangular amplitude diffraction grating. The other photon of the pair

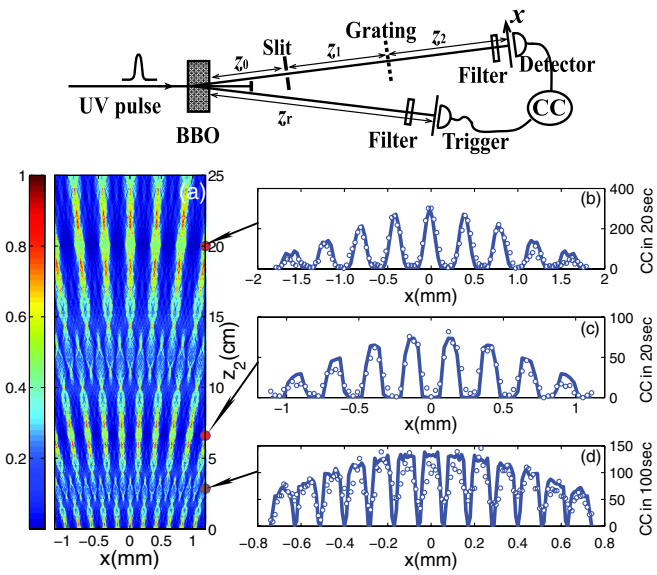

FIG. 1 (color online). Top: Experimental setup for first-order single-photon Talbot self-imaging. (a) Theoretical plot of the single-photon Talbot imaging carpet where x is the transverse position across the beam and z_2 the longitudinal position. The color bar denotes the relative intensity. (b)–(d) present the experimental results (open circles) of CCs for effective diffraction lengths: (b) $Z_a = z_T$ ($z_2 = 20$ cm), (c) $Z_a = (1/2)z_T$ ($z_2 = 6.6$ cm), and (d) $Z_a = (1/4)z_T$ ($z_2 = 2.85$ cm). The solid lines are theoretical curves. The red filled circles in (a) indicate the self-imaging positions corresponding to the experimental observations.

(the idler photon) is employed as a trigger. Both the signal and idler photons are spectrally filtered by an interference filter of 10 nm bandwidth centered at 800 nm and then detected by single-photon detectors (Perkin-Elmer SPCM-AQR-14). A time window of 4 ns is chosen to capture the coincidence counts.

For a periodic object of transmittance function $T(x_0)$ illuminated by a point source, the diffraction pattern in the detection plane under the paraxial approximation is given by

$$I(x) \propto \left| \int dx_0 T(x_0) \exp\left[\frac{i\pi}{\lambda Z_a} \left(x_0 - \frac{x}{1 + z_2/z_1} \right)^2 \right] \right|^2, \quad (1)$$

where z_1 and z_2 are the distances from the object to the source and the detector, respectively. Here $Z_a = \frac{z_1 z_2}{z_1 + z_2}$ represents the effective diffraction length, which is defined according to the Fresnel diffraction integral; x_0 and x are the transverse coordinates of the object and detection planes, respectively. If the object is a one-dimensional grating with slit width b and period d, then $T(x_0) = \sum_{n=-\infty}^{\infty} \mathrm{rect}[(x_0 - nd)/b]$. Here $\mathrm{rect}(u)$ is 1 for $|u| \leq 1/2$ and 0 for other values. In the case when $Z_a = mz_T$ (m is an integer), Eq. (1) reduces to

$$I(x) \propto \left| \sum_{n=-\infty}^{\infty} \mathrm{rect}\left[\frac{1}{b} \left(\frac{x}{1 + z_2/z_1} - nd \right) \right] \right|^2. \quad (2)$$

This represents classical first-order Talbot self-imaging with a magnification of $1 + z_2/z_1$. Figure 1(a) is a numerical simulation of a typical Talbot "carpet" pattern along the longitudinal coordinate z_2, obtained by using Eq. (1). The grating parameters are $b = 90$ μm and $d = 200$ μm, and the Talbot length is $z_T = 10$ cm for $\lambda = 800$ nm.

In our experimental setup, a single-slit aperture of width $a = 120$ μm is placed at a distance of $z_0 = 25$ cm from the BBO crystal and $z_1 = 20$ cm from the grating object. In fact, the Talbot effect for a point source is different from the case of plane waves. Experimentally, the point source can be avoided, for example, by using a lens between the slit and the grating. Here we employ the point source because it can be compared with the case in the ghost imaging configuration below. The single-photon detector is scanned across the signal beam and is triggered by the idler detector so that only coincidence counts (CCs) are recorded to avoid spurious counts and noise. When the signal photon detector is placed at distances of $Z_a = z_T$, $Z_a = (1/2)z_T$, and $Z_a = (1/4)z_T$, the CCs produce the self-imaging patterns shown in Figs. 1(b)–1(d), respectively. At a distance of one Talbot length, Fig. 1(b) shows the image of the grating with a magnification of 2. At one-half the Talbot length, however, Fig. 1(c) shows the same image but with a half-period shift and a magnification of 1.33. Moreover, at a quarter Talbot length the image period is reduced to a half. By taking into account the magnification of $1 + z_2/z_1 = 1.14$ in Fig. 1(d), the period of the pattern is $0.5 \times 1.14 \times 200 = 114$ μm.

Considering a limited width a of the single slit in the theoretical simulation, we derive the CCs in this scheme to be

$$R_D \propto \int_{-a/2}^{a/2} dx_s \left| \int dx_0 T(x_0) \exp\left[\frac{i\pi}{\lambda} \left(\frac{(x_0 - x_s)^2}{z_1} + \frac{(x - x_0)^2}{z_2} \right) \mathrm{sinc}\left(\frac{\pi a}{\lambda} \sin\phi \right) \right] \right|^2, \quad (3)$$

where ϕ is the diffraction angle satisfying $\sin\phi \approx \phi \approx x_0/z_1$ and x_s is the transverse coordinate in the single-slit plane. A single-slit diffraction factor (sinc function) is merged into the expression. The theoretical curves fit well with the experimental results.

The above discussion of the single-photon self-imaging effect pertains to the classical first-order Talbot effect. In the following, we study two kinds of the second-order quantum Talbot effect. One of the experimental setups is shown at the top of Fig. 2, which is a typical quantum ghost imaging configuration [15]. The entangled photon pairs are generated in the same way as that in Fig. 1. The signal photons pass through a grating to detector 1, and the idler

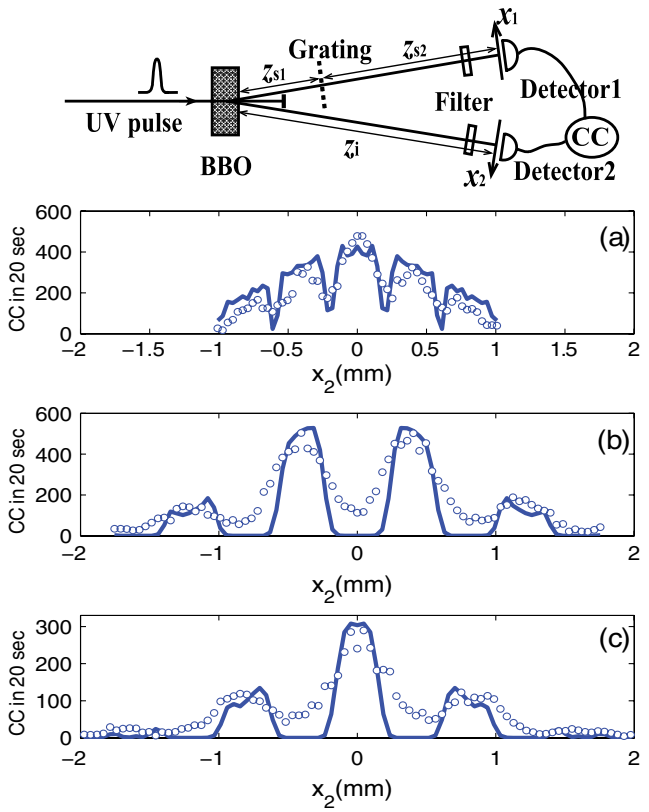

FIG. 2 (color online). Top: Experimental setup for two-photon second-order Talbot self-imaging in the ghost interference scheme. The open circles in (a)–(c) are the coincidence counts for effective diffraction lengths of (a) $Z_b = (1/4)z_T$ ($z_i = 12$ cm, $z_{s1} = 8$ cm, $z_{s2} = 20$ cm), (b) $Z_b = (1/2)z_T$ ($z_i = 25$ cm, $z_{s1} = 15$ cm, $z_{s2} = 40$ cm), and (c) $Z_b = z_T$ ($z_i = 25$ cm, $z_{s1} = 55$ cm, $z_{s2} = 80$ cm). The solid lines are theoretical curves.

photons travel freely to detector 2. Two interference filters are placed in front of the detectors. When detector 1 is fixed and detector 2 is scanned across the beam, coincidence counting between them can show ghost imaging.

In this scheme the effective diffraction length for the grating is given by $Z_b = z_{s2}(z_{s1} + z_i)/(z_i + z_{s1} + z_{s2})$ [13], where z_{s1} and z_i are the distances from the BBO crystal to the grating and detector 2, respectively, and z_{s2} is the distance from the grating to detector 1. The periodic structure can be enlarged by a magnification of $1 + (z_{s1} + z_i)/z_{s2}$. If one imagines detector 2 to be a source which emits a ray to the grating after reflection off the crystal, the present scheme is comparable with the previous one. In the experiment, the grating parameters are $b = 180$ μm and $d = 400$ μm, defining the Talbot length $z_T = 40$ cm for $\lambda = 800$ nm. When we take the effective diffraction lengths to be $Z_b = (1/4)z_T$, $Z_b = (1/2)z_T$, and $Z_b = z_T$, the experimental results are as shown in Figs. 2(a)–2(c), respectively. It is readily seen that in all three cases the magnification is two, while the image period is 400 μm in Fig. 2(a) and 800 μm in Figs. 2(b) and 2(c). In the theoretical simulation, a Gaussian intensity profile with a full width of 1.8 mm for the source is taken. The experimental data (open circles) basically agree with the theoretical curves (solid lines), thus verifying the theoretical analysis of the second-order Talbot effect with entangled light.

We now explore the two-photon subwavelength Talbot effect, in which a periodic object is illuminated by a biphoton source. The experimental setup is sketched at the top of Fig. 3. The 400 nm pulsed beam is used to pump a $5 \times 5 \times 2$ mm type-II cut BBO crystal to generate collinear orthogonally polarized photon pairs. The grating is placed immediately after the crystal. The slit, polarizing beam splitter, and coincidence circuit work together as a two-photon detector. For convenience, instead of moving the two detectors, we rotate mirror M to "scan" the diffraction pattern across the detector surfaces [16]. The time window for the coincidence counts is 2 ns.

In this scheme we use a grating with $b = 120$ μm and $d = 300$ μm, corresponding to a first-order Talbot length of $z_T = 22.5$ cm for $\lambda = 800$ nm. Let Z_c be the distance between the grating and the slit (i.e., $z_{c1} + z_{c2}$ in Fig. 3.). For the three cases of $Z_c = (1/2)z_T$, $Z_c = z_T$, and $Z_c = 2z_T$, self-imaging patterns are observed as shown in the left part of Figs. 3(a)–3(c), respectively. The experimental data and theoretical curves are indicated by open circles and solid lines, respectively. In the numerical simulation, we assume a Gaussian intensity profile with a full width of 1.0 mm. For comparison, the right part shows the corresponding images when the two-photon source is replaced by a coherent beam of the same wavelength.

It has been known that two-photon interference can exhibit subwavelength resolution such that the spacing between the interference fringes is reduced to half of that

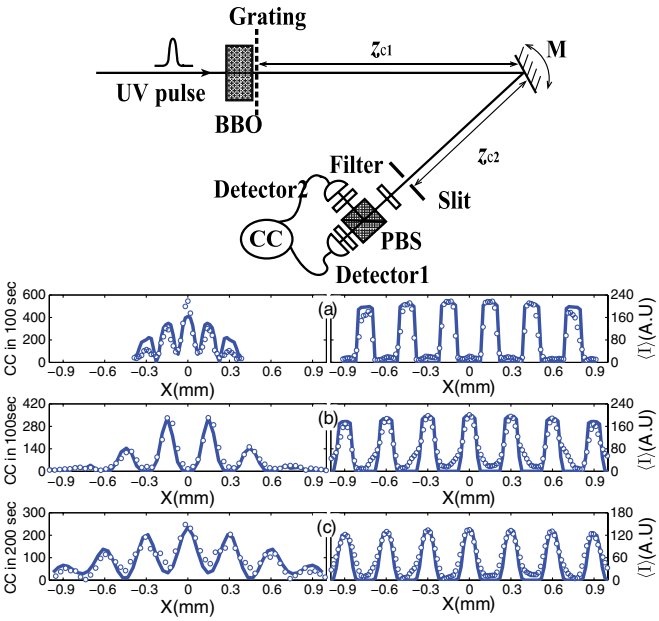

FIG. 3 (color online). Top: Experimental setup for two-photon second-order Talbot self-imaging in the quantum lithography scheme. The open circles are experimental data observed for effective diffraction lengths of (a) $Z_c = (1/2)z_T = 11.25$ cm, (b) $Z_c = z_T = 22.5$ cm, and (c) $Z_c = 2z_T = 45$ cm. Left and right parts correspond to the entangled two-photon source and the coherent light source, respectively. The solid lines are theoretical curves.

for one-photon interference [16,17]. However, the experiment results in Fig. 3 show different phenomena for the two-photon Talbot effect. Comparing the interference patterns observed for the two-photon and the coherent sources, we find that when $Z_c = (1/2)z_T$, the fringe period for the former is 150 μm, which is half of that for the coherent source. However, for $Z_c = z_T$ and $Z_c = 2z_T$, the image periods for both sources are the same as in the original grating. In particular, the two-photon self-images undergo a half-period shift for $Z_c = z_T$ but not for $Z_c = 2z_T$.

If we define the two-photon Talbot length as $Z_T = 2d^2/(\lambda/2) = 2z_T$, the experimental results can be properly understood. The left images of Fig. 3(a)–3(c) correspond to 1/4, 1/2, and one two-photon Talbot length Z_T, respectively. Comparing these patterns with the classical Talbot images at the corresponding Talbot lengths, we find that the image resolution is not improved by a factor of 2, while the Talbot length is doubled.

We verify the above understanding with a brief theoretical analysis. The two-photon amplitude for a two-photon entangled state $|\psi\rangle$ is written as

$$\langle 0|E_1^{(+)}(x_1)E_2^{(+)}(x_2)|\psi\rangle \propto \int dx_0 T^2(x_0) \exp\left\{\frac{i\pi}{\lambda Z_c}[(x_1 - x_0)^2 + (x_2 - x_0)^2]\right\}, \quad (4)$$

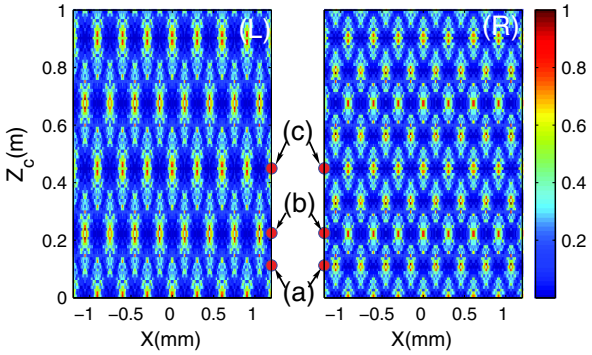

FIG. 4 (color online). Talbot self-imaging carpets plotted for a grating illuminated by (left) a two-photon entangled source and (right) a classical plane wave source. The red filled circles indicate the three self-imaging positions of Fig. 3.

where $E_1^{(+)}(x_1)$ and $E_2^{(+)}(x_2)$ are the positive frequency parts of the electric field in the detection plane. The two-photon process features diffraction for $T^2(x_0)$ instead of $T(x_0)$. Here our rectangular mask object satisfies $T^2(x_0) = T(x_0)$, so by setting $x_1 = x_2 = x$ in Eq. (4), we obtain

$$\langle 0|E_1^{(+)}(x)E_2^{(+)}(x)|\psi\rangle \propto \int dx_0 T(x_0) \exp\left\{\frac{i\pi}{\lambda(Z_c/2)}(x-x_0)^2\right\}. \tag{5}$$

If we regard the effective diffraction length as $Z_c/2$, Eq. (5) is equivalent to the classical case. Hence we define the two-photon Talbot length to be $Z_T = 2z_T$, which has incorporated the two-photon subwavelength feature.

In the far-field limit when the quadratic phase factor in the integration can be neglected, the factor 2 can also be included into the transverse position $2x$. As a result, the resolution of a two-photon diffraction pattern is doubled at the same distance as a one-photon process. But this is not the case for near-field diffraction.

With the same parameters for the grating and wavelength as in the present scheme, we plot the near-field Talbot carpets simulations in Figs. 4 (left) and (right) for the two-photon and one-photon cases, respectively. We do not see the transverse resolution improved for the two-photon case. Instead, the carpet is stretched twice as far along the longitudinal direction.

In summary, we have experimentally observed quantum Talbot images with both single photons and entangled photon pairs. The revival distance of two-photon Talbot imaging is demonstrated to be twice the usual classical Talbot length, and there is no net improvement in the resolution, due to the near-field effect of Fresnel diffraction; this is in contrast to previous two-photon quantum lithography experiments. We attribute this phenomenon to multiphoton near-field diffraction, which should be considered in quantum lithography using self-imaging. It is to be hoped that our results will be of value not only to quantum metrology and scanning near-field optical microscopy but also to other quantum optical technologies.

This work was supported by the National Natural Science Foundation of China (Grants No. 10825416, No. 10874019, No. 60708009, and No. 60978002), the National Program for Basic Research in China under Grants No. 2007CB613205 and No. 2010CB922904, and the National High Technology Research and Development Program of China (No. 2011AA120102).

*To whom all correspondence should be addressed.
zhangxd@bnu.edu.cn

[1] H. F. Talbot, Philos. Mag. **9**, 401 (1836).
[2] L. Rayleigh, Philos. Mag. **11**, 196 (1881).
[3] K. Patorski, in *Progress in Optics*, edited by E. Wolf (North-Holland, Amsterdam, 1989), Vol. 27, pp. 1–108.
[4] M. S. Chapman, C. R. Ekstrom, T. D. Hammond, J. Schmiedmayer, B. E. Tannian, S. Wehinger, and D. E. Pritchard, Phys. Rev. A **51**, R14 (1995).
[5] S. J. Wu, E. Su, and M. Prentiss, Phys. Rev. Lett. **99**, 173201 (2007).
[6] L. Deng, E. W. Hagley, J. Denschlag, J. E. Simsarian, M. Edwards, C. W. Clark, K. Helmerson, S. L. Rolston, and W. D. Phillips, Phys. Rev. Lett. **83**, 5407 (1999).
[7] R. Iwanow, D. A. May-Arrioja, D. N. Christodoulides, G. I. Stegeman, Y. Min, and W. Sohler, Phys. Rev. Lett. **95**, 053902 (2005).
[8] T. Weitkamp, B. Nöhammer, A. Diaz, and C. David, Appl. Phys. Lett. **86**, 054101 (2005); F. Pfeiffer *et al.*, Nature Mater. **7**, 134 (2008).
[9] Y. Zhang, J. Wen, S. N. Zhu, and Min Xiao, Phys. Rev. Lett. **104**, 183901 (2010).
[10] X. B. Song, J. Xiong, X. D. Zhang, and K. G. Wang, Phys. Rev. A **82**, 033823 (2010).
[11] K. H. Luo, X. H. Chen, Q. Liu, and L. A. Wu, Phys. Rev. A **82**, 033803 (2010).
[12] I. Vidal, S. B. Cavalcanti, E. J. S. Fonseca, and J. M. Hickmann, Phys. Rev. A **78**, 033829 (2008).
[13] K. H. Luo, J. Wen, X. H. Chen, Q. Liu, M. Xiao, and L. A. Wu, Phys. Rev. A **80**, 043820 (2009); **83**, 029902(E) (2011).
[14] C. H. Raymond Ooi and B. L. Lan, Phys. Rev. A **81**, 063832 (2010).
[15] T. B. Pittman, Y.-H. Shih, D. V. Strekalov, and A. V. Sergienko, Phys. Rev. A **52**, R3429 (1995); D. V. Strekalov, A. V. Sergienko, D. N. Klyshko, and Y.-H. Shih, Phys. Rev. Lett. **74**, 3600 (1995).
[16] E. J. S. Fonseca, C. H. Monken, and S. Pádua, Phys. Rev. Lett. **82**, 2868 (1999); M. D'Angelo, M. V. Chekhova, and Y.-H. Shih, Phys. Rev. Lett. **87**, 013602 (2001).
[17] A. N. Boto, P. Kok, D. S. Abrams, S. L. Braunstein, C. P. Williams, and J. P. Dowling, Phys. Rev. Lett. **85**, 2733 (2000).
[18] See also M. I. Kolobov, Rev. Mod. Phys. **71**, 1539 (1999); A. Gatti, E. Brambilla, and L. A. Lugiato, Prog. Opt. **51**, 251 (2008).